Microstructural and mechanical properties of silica–PEPEG polymer composite xerogels

ARTICLE *in* ACTA MATERIALIA · NOVEMBER 2006

Impact Factor: 4.47 · DOI: 10.1016/j.actamat.2006.06.055

Available online at www.sciencedirect.com
ScienceDirect
Acta Materialia 54 (2006) 5231–5240
Acta MATERIALIA
www.actamat-journals.com

Microstructural and mechanical properties of silica–PEPEG polymer composite xerogels

Manish M. Kulkarni [a], Rajdip Bandyopadhyaya [a], Bishakh Bhattacharya [b], Ashutosh Sharma [a,*]

[a] *Department of Chemical Engineering, Indian Institute of Technology, Kanpur 208016, UP, India*
[b] *Department of Mechanical Engineering, Indian Institute of Technology, Kanpur 208016, UP, India*

Received 27 February 2006; received in revised form 29 June 2006; accepted 29 June 2006
Available online 14 September 2006

Abstract

We prepared and characterized silica–polyethylene-*block*-polyethylene glycol (PEPEG) nanocomposite xerogels and investigated the role of addition of the elastic PEPEG oligomer in a brittle porous silica matrix by relating microstructure to mechanical properties. For PEPEG < 7 wt.%, the oligomer fills smaller pores in the silica matrix; but, as evidenced by atomic force microscopy and Fourier transform infrared spectroscopy, PEPEG partially disrupts matrix formation at higher concentrations. Consequently the pore size distribution shifts towards larger sizes and the specific surface area of the composite decreases. The toughness increases continuously with PEPEG addition. The elastic modulus of the composite increases twofold for 7 wt.% PEPEG, but decreases on further addition of PEPEG. Microhardness and structural loss factor also show a similar optimum for PEPEG at around 5–7 wt.%. The analytical and empirical models agree with the experimental modulus values for lower PEPEG addition, but fail to explain the maximum because of their inability to capture the observed microstructural changes in the composite structure.

Keywords: Polymer–silica xerogels; Silica–PEPEG composite; Nanocomposites; AFM

1. Introduction

Addition of polymers in an inorganic matrix improves elastic properties of the intrinsically brittle silica network [1–3], conductivity of ionic solid-state conductors [4], dispersion of nanocrystals in the matrix and modification of dielectric constant [5]. However, the exact relationship between structural modifications of the matrix and various physical and mechanical properties of the resultant composites due to the addition of a second phase has not been elucidated in all cases.

The objective of the present study is to analyze various microstructural, physical and mechanical changes in a silica xerogel network on addition of an elastic polymer like polyethylene-*block*-polyethylene glycol (PEPEG). As the average molecular weight of PEPEG used for the present study is only 1400, we refer to it as an oligomer. With a PEPEG loading as small as 7 wt.%, we could make a composite that is four times tougher and with about twice the compressive modulus, compared to pure silica. Apart from the sample-specific finite element method (FEM) [6], more general analytical and empirical models of Hashin–Shtrikman (H–S) [7] and Halpin–Tsai (H–T) [8] have been successfully applied for many multiphase physical composites for predicting various properties [9–11]. In the present case, both the H–S and H–T models predict that addition of oligomer should improve the elasticity of the composite. The model predictions compare well with our experimental observations for lower oligomer addition (<7 wt.%). However, as demonstrated here (above 7 wt.% PEPEG in this case), the structure–property relationship can be complex, especially in the case of chemical

* Corresponding author. Tel.: +91 512 259 7026; fax: +91 512 259 0104.
E-mail address: ashutos@iitk.ac.in (A. Sharma).

1359-6454/$30.00
doi:10.1016/j.actamat.2006.06.055

composites, where the second phase alters the physicochemical properties of the primary phase by actively reacting with it. For addition of 7 wt.% oligomer, the elastic modulus of the composite was highly underestimated by both the models. Moreover, when the oligomer loading was increased further, the modulus of the composite decreased, instead of increasing, as predicted by these models. Using analytical techniques like pore size distribution (Brunauer, Emmett and Teller (BET) surface area and Barrett, Joyner and Halenda (BJH) pore size distribution measurements), Fourier transform infrared spectra (FTIR) and atomic force microscopy (AFM), we explain the structural modifications in this sol–gel composite and their impact on the observed mechanical properties. A study of the vibration damping properties of the composites was also carried out.

2. Experimental

Sol–gel processing is found to be especially useful for preparing nanocomposites, because growth of the base matrix and structural properties can be tuned easily by changing various parameters such as pH, precursor/solvent molar ratio, hydrolysis and condensation rates, etc. [12]. Polymers have been incorporated into silica matrices either by choosing an appropriate common solvent for both silica and polymer precursors during the preparation of the sol or by first preparing silica gels and then replacing the pore solvent of the gels by polymer–solvent mixtures (derivatization) [13,14].

In the present work, sol–gel processing was used to prepare silica and PEPEG nanocomposites. PEPEG block copolymer was selected because it is soluble in alcohol–water mixtures that are commonly used to prepare organometallic precursor-based silica gels. As reported in the literature, the polyethylene chains have higher compressive modulus (~245 MPa [15] as compared to 20–100 MPa for pure silica xerogels [16]). Also, the labile glycol group present in the ethylene glycol monomer can bind the PEPEG chains to the silica network, on reaction with the surface –OH groups of silica [5].

Silica xerogel composites were prepared by a two-step acid–base catalyzed sol–gel processing [17–19]. Ethanol (EtOH)-diluted tetraethoxysilane (TEOS; Fluka, purum grade, 98.0% (GC)) was partially hydrolyzed by adding (under-stoichiometric) 2% aqueous solution of HCl with stirring and kept hermitically closed. After 24 h, PEPEG (Aldrich, $M_n = 1400$) of predetermined amount was added to this sol and the mixture was stirred for about 20 min until the oligomer granules dissolved in the sol. Subsequently further water was added to the mixture in the form of a base catalyst (1 M NH_4OH), so the final molar ratios of TEOS:EtOH:H_2O was 1:6.9:9.4. The PEPEG content with respect to TEOS was increased from 0 to 10 wt.%. It was observed that above 10 wt.% of PEPEG, monolithic xerogels could not be obtained. The resulting sol was poured into polypropylene moulds for gelation took place at room temperature within 10 min. The gels were dried slowly in an oven at three successive temperatures to preserve the monolithic composite sample of large dimensions. Initially they were heated at 50 °C for 4 days. The gels shrunk to about 70% of their original volume during this period. Subsequently, the gels were transferred to glass Petri dishes and heated at 100 °C for 12 h followed by heating at 150 °C for an additional 12 h. The shrinkage of the gels after the initial heating at 50 °C was negligible.

The BET specific surface area and BJH pore size distribution measurements were carried out using a Coulter SA-3100 surface analyzer. Tapping mode AFM (TMAFM) was used to study the topography and phase features of the xerogel surface. All AFM measurements were carried out using a PicoSPM II (Molecular Imaging, USA) instrument operated in tapping mode. Measurements were performed at a setpoint amplitude A_{sp} of $0.85A_o$ (free oscillation amplitude). The data analysis was carried out using the Picoscan software. Micromasch SPM cantilevers (NSC36/Cr–Au) with resonance frequencies of the order of 170 kHz and spring constants between 0.4 and 5 N/m were used for these experiments.

The functional groups of the xerogel composites were studied using FTIR spectroscopy (Bruker FTIR) of the dried samples by forming pellets of KBr powder and xerogel sample. The microhardness of the xerogel composites was measured using a Leica VMHT 30 M microhardness testing instrument samples with dimensions of 25 mm × 15 mm × 3 mm were cut for compression modulus testing performed using a Materials Test System (MTS 810). In order to estimate the error in the values of microhardness, toughness and compressive modulus, these measurements were repeated for three to five different sets of xerogel samples having the same composition, wherever possible.

3. Results and discussion

3.1. Microstructural observations

The effect of oligomer addition on the structural properties of the composite xerogel was studied by specific (sp.) surface area and pore size distribution measurements.

BET specific surface area (S) and specific pore volume (V_v) of the samples are plotted as a function of PEPEG concentration in Fig. 1 (note that some of the error bars are not visible in Figs. 1 and 2 as they are smaller than the data symbols). It is observed that as the amount of PEPEG increases from 0 to 10 wt.%, the specific surface area decreases from 604 to 306 m^2/g, while the specific pore volume increases from 0.14 to 0.30 cm^3/g and then decreases slightly to 0.25 cm^3/g. The specific surface area decreases because the oligomer fills some of the pores in the silica matrix, while the increase in the specific pore volume is related to the pore size. Fig. 2 shows the plot of pore size distribution (PSD) as a function of pore diameter. It is

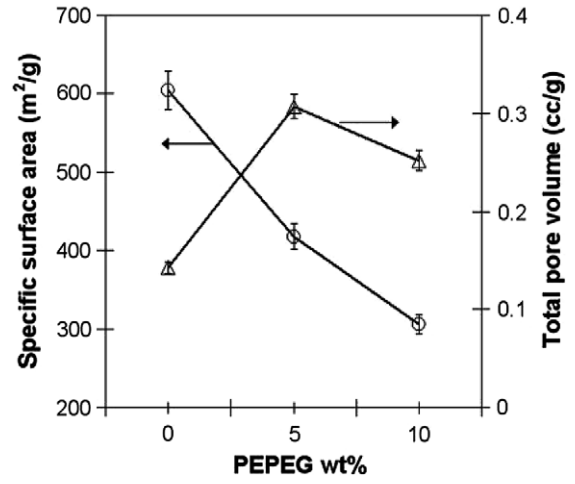

Fig. 1. Surface area and pore volume of xerogel composites with different PEPEG contents.

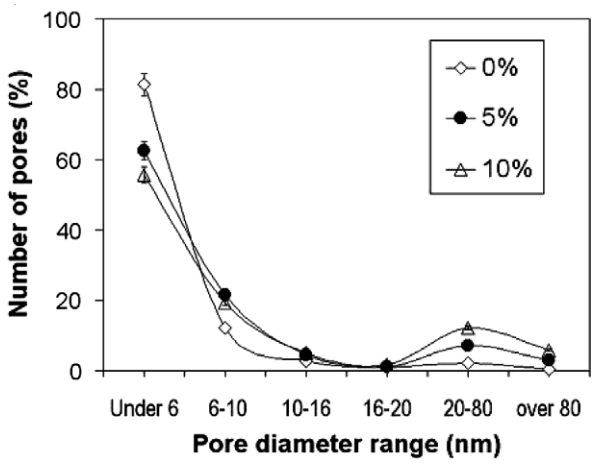

Fig. 2. Pore size distribution of pure silica (0 wt.%) and composite xerogels (5 and 10 wt.% PEPEG).

seen that as the amount of PEPEG increases from 0 to 10 wt.%, the PSD shifts slightly towards larger pores. Simultaneously, the percentage of pores with pore diameters smaller than 10 nm decreases from 93% to 74%, while that of pores having pore diameters larger than 20 nm increases from 2.5% to 18%. This shift in pore size indicates that the silica network cross-linking is affected by the addition of polymer. These structural changes are discussed in detail later. Using the pore volume (V_v), bulk density (ρ_b) and skeletal density (ρ_s), the porosity (ϕ) of the pure and composite xerogels was calculated from the following relations [20]:

$$\rho_s = [(1/\rho_b) - V_v]^{-1} \quad (1)$$

$$\phi = [1 - (\rho_b/\rho_s)] \quad (2)$$

These values for samples prepared using 0, 5 and 10 wt.% PEPEG are listed in Table 1. Even though porosity increased with the addition of oligomer, the bulk density of the xerogels did not change significantly and was found to be around 1 g/cm^3.

The above observations suggest that an increased amount of PEPEG leads to a more open-structured composite matrix, with around 25–33% of pores filled by PEPEG.

When PEPEG is added to the sol phase, it can either remain trapped in the silica matrix or react with –OH groups present on the pore wall surface according to the following reaction [5]:

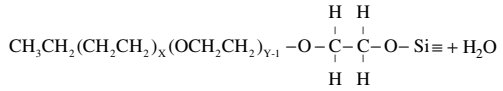

$$CH_3CH_2(CH_2CH_2)_X(OCH_2CH_2)_YOH + OH-Si\equiv \rightarrow CH_3CH_2(CH_2CH_2)_X(OCH_2CH_2)_{Y-1}-O-\underset{H}{\overset{H}{C}}-\underset{H}{\overset{H}{C}}-O-Si\equiv + H_2O \quad (3)$$

However, it may be noted that, during the preparation of the gel, oligomer and base catalyst were added 24 h after the addition of the acid catalyst to the sol, so the sol mainly consists of silicic acid [$Si(OH)_4$] before addition of the oligomer [21]. Once the base catalyst is added to the sol, condensation reactions of silicic acid groups are much faster compared to condensation between Si–OH and R–OH groups of oligomer [22a]. This is because the oxygen atom of the silanol (Si–OH) group is more electron-rich than the oxygen atom of the alcohol (R–OH), which makes the former a better nucleophile than the latter. Therefore, formation of ≡Si–O–Si≡ matrix though condensation of Si–(OH) groups is more favored even after addition of <7 wt.% PEPEG to the sol, as discussed for the FTIR investigation below.

Fig. 3 shows FTIR spectra of the pure silica xerogel, pure PEPEG and composite xerogel samples. It is seen that as the amount of PEPEG increases, the intensity of the absorption bands at 2865 and 2930 cm^{-1} increases. These correspond to the symmetrical and asymmetrical stretching of the CH_2 bonds. The broad absorption band around 1100 cm^{-1} and the smaller bands around 800 and 400 cm^{-1} correspond to various vibration modes of the Si–O–Si bonds [23]. The decrease in the magnitudes of these was more pronounced compared to the increase in C–H absorption bands with increasing PEPEG concentration. This decrease in the otherwise very prominent absorption bands of Si–O–Si bonds indicates that as the amount of oligomer in the sol increases, the formation of silica matrix is hindered by the larger amount of PEPEG. The broad absorption bands of O–H around 3500 and 1650 cm^{-1} decreased with addition of more oligomer. This decrease is the combined effect of condensation of Si–OH groups with the reactive –OH group (as shown in Eq. (3)) of PEPEG monomer and increased pore size of the composite with increase in PEPEG content. The latter leads to better evaporation of the ethanol–water solvent trapped in the gel matrix during the drying process.

Even though the condensation reaction between Si–OH and PEPEG is possible, PEPEG cannot act as a bridging element to complete the matrix. This argument is consistent

Table 1
Measured BET surface area, pore volume and porosity as a function of PEPEG content

PEPEG (wt.%)	Specific surface area, S (m^2/g)	Specific pore volume, V_v (cm^3/g)	Bulk density, ρ_b (g/cm^3)	Skeletal density, ρ_s (g/cm^3)	Porosity, ϕ
0 (pure silica)	604	0.14	1.04	1.23	0.15
5	418	0.31	1.00	1.46	0.31
10	306	0.25	1.11	1.55	0.28

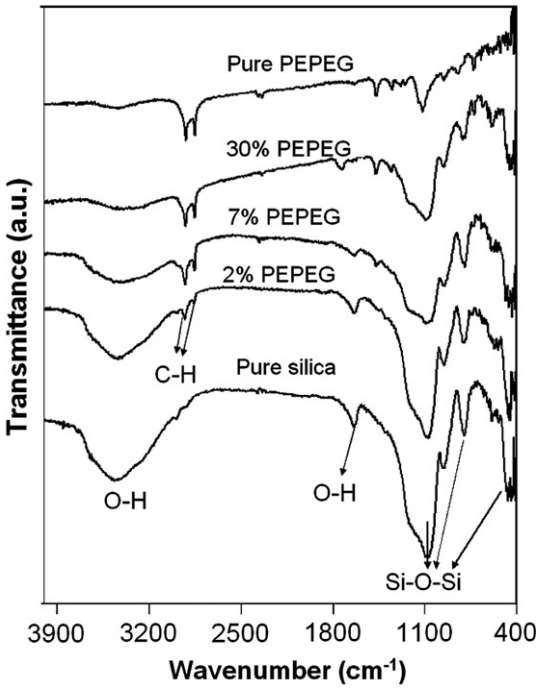

Fig. 3. FTIR spectra of silica–PEPEG composites.

with the observation that monolithic xerogel samples could not be obtained above 10 wt.% of PEPEG. However, due to the overlap of the vibration modes of Si–O–C (1110 and 1190 cm^{-1}) and Si–O–Si (around 1100 cm^{-1}) [5], it could not be established from the FTIR absorption spectra whether the PEPEG reacts with the silica network actively or if it just remains trapped in the matrix.

To estimate how the oligomer penetrates and affects the microstructure of the composite, we calculated the total number of Si–OH reactive sites in the silica matrix, where the oligomer can react and thereby chemically bond to the network. This is obtained by multiplying the measured specific surface area of each of the composites with the about 5 surface –OH groups per nm^2 surface area of silica gel, as measured from TEOS precursor [22a]. As is seen in Table 2, this number is of the order of 10^{12} per gram of composite. In comparison, there is one –OH group per PEPEG monomer and from the known amount of PEPEG added to the sol, the number of labile –OH groups in PEPEG per gram of composite was calculated to be around 10^{21}. Therefore, even if it is assumed that glycol–hydroxyl reactions become dominant after gel formation, most of the oligomers remain unreacted. Further, one can also estimate the volume occupied by the PEPEG molecules to estimate how much void volume can be filled by the oligomer chains. It was assumed that PEPEG oligomer ($M_n \sim 1400$) remains fully stretched or uncoiled, and hence the average chain length of the monomer is ~7 nm. The volume occupied by these oligomer chains is given in the last column of Table 2. This is much smaller than the void volume (V_v) of the composite given in Table 1. Moreover, the oligomer chains tend to coil and hence further decrease several-fold the estimated volume. Thus, even if all the oligomer chains penetrate the pore, a large volume fraction of the pores remains unfilled. From the above discussion, it can be summarized that most of the pores remain unfilled and a large fraction of the oligomer added to the sol remains unreacted within the composite matrix. The TMAFM studies give further evidence for the above arguments.

Topographic and phase contrast images of pure silica and composite xerogels obtained using TMAFM are shown in the left and right panels of Figs. 4 and 5, respectively. It is clearly seen from the topographic images that as the amount of PEPEG increases from 0 to 10 wt.% (Fig. 4a–c), the mean sizes of individual particles of the silica network continuously increase from 80 to 120 nm. The left panel of Fig. 4a shows that for pure silica, the network consists of uniform silica particles of ~80 nm diameter (area A). The area marked B in this image shows a typical empty pore. The corresponding phase image in the right panel of Fig. 4a shows only one gray shade indicating the presence of only silica phase. This is because the pores are not seen as a separate phase in the phase scan (of Fig. 4a), due to the presence of other silica particles lying beneath the pores.

Table 2
Estimated number of reactive –OH groups of silica and PEPEG molecules and volume occupied by PEPEG molecules

PEPEG (wt.%)	No. of Si–OH groups per gram of composite xerogel ($\times 10^{-12}$)	No. of –OH groups of PEPEG per gram of composite xerogel ($\times 10^{-21}$)	Total volume occupied by uncoiled PEPEG molecules (cm^3/g)
0 (pure silica)	3.02	–	–
5	2.09	2.06	0.082
10	1.53	4.12	0.1640

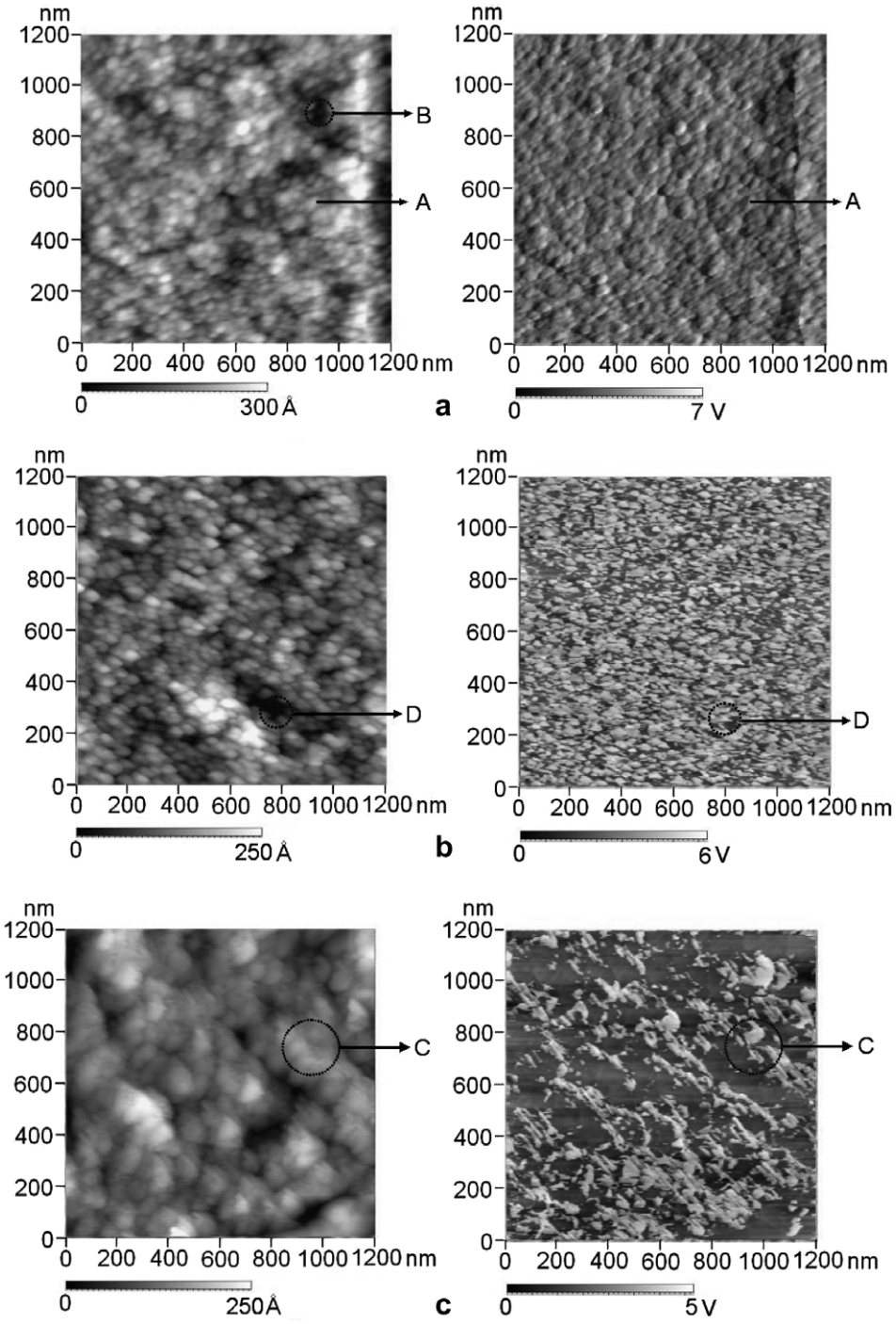

Fig. 4. TMAFM images of silica–PEPEG composite xerogels: (a) pure silica; (b) silica with 7 wt.% PEPEG; (c) silica with 10 wt.% PEPEG. Topographic and phase scans are in left and right panels, respectively. Symbols are defined as: A, silica particle; B, empty pore; C, PEPEG chains on silica particles; D, pore filled with PEPEG.

However, for 7 and 10 wt.% PEPEG composites (Fig. 4b and c, respectively), both silica and PEPEG phases are seen clearly in topography and phase scans. In these phase images, the dominant light-gray region corresponds to silica and the dark-gray region corresponds to PEPEG. In Fig. 4b, the topographic scan shows a typical pore within the area marked D. However, comparing this region in the corresponding phase scan, it is clear that this pore is filled by PEPEG, as the phase scan shows both the silica and PEPEG phases. With an increase in the amount of PEPEG, it not only fills some of the pores but also increasingly covers some silica particles as seen from Fig. 4c. Here the topographic scan shows chains of particles (area marked C). These are composed of both silica and PEPEG as seen from the corresponding phase scan. In particular, for 10 wt.% PEPEG, as the condensation

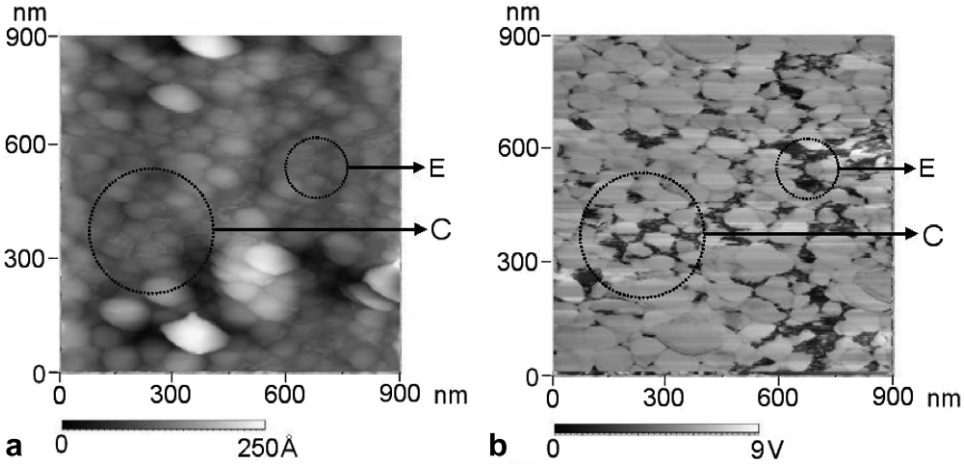

Fig. 5. TMAFM images of silica with 7 wt.% PEPEG composite. Topographic and phase scans are in left and right panels, respectively. Note the PEPEG phase distribution, which is dominant in pores (area marked D) and neck region of the silica particles (area marked C). Incomplete linking of silica chains due to the PEPEG is marked by E.

of ≡Si–OH species between themselves is much faster than condensation of glycol (from PEPEG) with Si–OH, silica chain formation first takes place to a significant extent. It is expected that most of the PEPEG wraps the silica chains only later. This process of wrapping of silica chains in turn prevents their interlinking to some extent and gives rise to larger interparticle pores. This is shown in Fig. 4c.

Fig. 5 shows topography and phase scans with a higher resolution for a composite with 7 wt.% PEPEG. Here the relative phase distribution of PEPEG between silica and pores is clearly visible. A comparison of the phase and topographic images shows that the oligomer partly fills some of the pores and also partitions in the "neck" region between two silica particles (area marked C). Necks between two adjoining particles have a negative radius of curvature. Solubility of material is especially low in this region leading to oligomer accumulation [22b]. This results in a reduction of the net curvature of the solid phase. Accumulation in the neck region adds to the strength and stiffness of the network to some extent [24].

Some regions in the phase scan of Fig. 5 (e.g. area E) clearly show the presence of PEPEG between two nearby silica chains, while the corresponding topographic scan does not show any pores between these chains. This process prevents cross-linking of these particular silica chains, which results in a decrease in the strength of the composite. This effect would be more significant especially at higher PEPEG contents.

Based on these observations, schematic diagrams showing the microstructure of the pure and composite xerogels are given in Fig. 6. The spherical silica particles link each other through Si–O–Si bonds and the oligomeric chains partly fill some of the pores of this network and partly remain trapped in the matrix. These different phases are shown in gray shades in the schematic.

3.2. Mechanical properties of the xerogel composites

Xerogel samples having dimensions of 25 mm × 15 mm × 3 mm were subjected to compression load and the corresponding load vs. deflection plots were obtained. From these data the resultant stress vs. strain curves were plotted. The Young's modulus (E_c) of the composite was calculated from the average of the slope of the stress–strain curves for various samples with identical compositions and is shown as a function of PEPEG concentration in Fig. 7. E_c increases from ~87 MPa for 0 wt.% to ~157 MPa for 7 wt.% and decreases again to ~98 MPa with further addition of PEPEG. This observation is similar to the case of silica–PEG composite aerogels reported by Martin et al. [3], where the elastic modulus of the composites increased from 4.4 to 6.4 MPa with an increase in PEG from 0 to 0.01 wt.% and decreased to 0.92 MPa with further increase in PEG to 0.04 wt.%. In the present case, E_c of the composite having 7 wt.% PEPEG is a maximum probably because of the optimum configuration of oligomer, where slight retardation of the silica network formation is compensated by reinforcement of the silica network due to filling of the pores by PEPEG. As seen from the TMAFM scan (Fig. 4b), most of the pores are filled by PEPEG at a PEPEG concentration of 7 wt.%, but at this concentration, the silica network remains largely intact. In contrast, at 10 wt.% PEPEG, although PEPEG is present in many of the pores, the silica network is partially disrupted by the oligomer chains, as seen from Fig. 4c and supported by the FTIR observations. Thus, the Young's modulus of the silica–PEPEG xerogel composite decreases above 7 wt.% PEPEG.

Modeling the mechanical properties of composites prepared by a chemical route like sol–gel processing is a difficult task due to the complex microstructural changes. No particular model is found to predict the properties of such composites under all conditions. However, H–S bounds

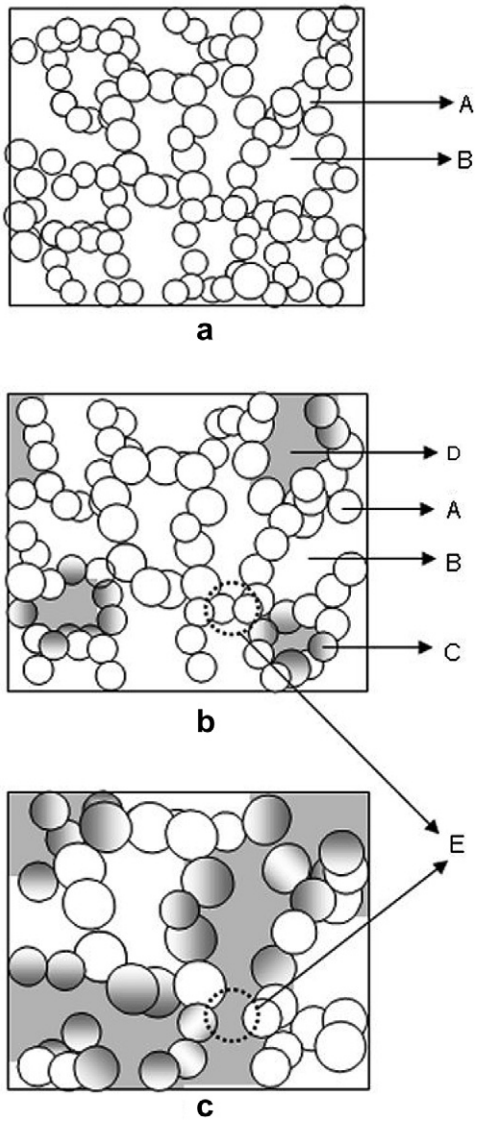

Fig. 6. Schematic representation of different silica–PEPEG composite xerogels: (a) pure silica; (b) silica with low PEPEG content; (c) silica with high PEPEG content. The increasing pore and particle sizes from (a) to (c) are not to scale. Symbols are defined as: A, silica particle; B, empty pore; C, PEPEG chains on silica particles; D, pore filled with PEPEG; E, incomplete linking of silica chains due to PEPEG.

and the H–T model were reported to be partially successful analytical and empirical models within certain limits, at least for simple configurations of constituent phases [9–11,24]. These models can be applied to a multiphase system where the ratio of elastic modulus of the primary phase (i.e. silica matrix $E_s = 87$ MPa) to the inclusion (i.e. PEPEG, $E_p \sim 250$ MPa) is of the order of the aspect ratio (α) of the inclusion [26]. We have observed from the TMAFM scans that PEPEG chains completely fill some of the nearly spherical pores in the silica matrix. Hence, α is of the order of about 1, which is approximately of the same order as the E_s/E_p ratio (=0.348). Therefore, we compared the experimental results with the theoretical values of elastic modulus (E_c) of composites calculated using H–T equations as well as H–S bounds.

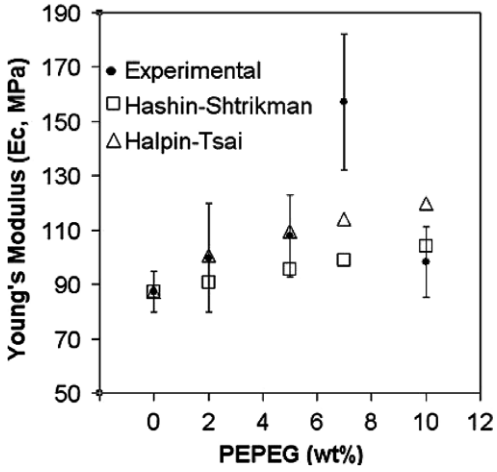

Fig. 7. Comparison of experimental values of Young's modulus (E_c) of silica–PEPEG composite with that of E_c calculated using H–S bound and H–T fits. The errors in the experimental data are estimated from measurements of at least four different samples of identical composition.

In the H–T formulation, the composite modulus of elasticity (E_c) is expressed as

$$\frac{E_c}{E_s} = \frac{1 + \xi_p \eta V_p}{1 - \eta V_p} \tag{4}$$

where

$$\eta = \frac{E_p/E_s - 1}{E_p/E_s + \xi_p}$$

V_p is the PEPEG volume fraction and the fitting parameter ξ was chosen to be $\xi(G_i) = K_i/(K_i + 2G_i)$ and $\xi(K_i) = G_i/K_i$ (i = s for silica and p for PEPEG) as reported by Wall [25]. However, the H–T formulation is an empirical model. A more rigorous analytical model could be obtained using the H–S upper and lower bounds of elasticity modulus, where the lower and upper bounds of bulk (K_l, K_u, respectively) and shear (G_l, G_u, respectively) modulus are initially calculated using the following equations:

$$K_l = K_p + V_s \left[\frac{1}{K_s - K_p} + \frac{V_p}{K_p + G_p} \right]^{-1} \tag{5}$$

$$K_u = K_s + V_p \left[\frac{1}{K_p - K_s} + \frac{V_s}{K_s + G_s} \right]^{-1} \tag{6}$$

$$G_l = G_p + V_s \left[\frac{1}{G_s - G_p} + \frac{V_p(K_p + 2G_p)}{2G_p(K_p + G_p)} \right]^{-1} \tag{7}$$

$$G_u = G_s + V_p \left[\frac{1}{G_p - G_s} + \frac{V_s(K_s + 2G_s)}{2G_s(K_s + G_s)} \right]^{-1} \tag{8}$$

where V_s and V_p are volume fractions of silica matrix and PEPEG, respectively. K_s, K_p and G_s, G_p are the bulk and shear modulii of silica matrix and PEPEG, respectively. The lower and upper bounds of Young's modulus of the composite were then calculated using the relation

$$E = \frac{9K}{(1 + 3K/G)} \tag{9}$$

The average value of lower and upper bounds of elastic modulus of composite (E_c) is plotted against PEPEG concentration in Fig. 7.

At a low PEPEG content (<7 wt.%), both the models fit well with the observed E_c values within experimental error bounds. However, the fitted curves do not follow the experimental observations, especially for PEPEG > 5 wt.%, as seen in Fig. 7. Hence, in the H–T model, E_c was also calculated for various arbitrary values of ξ, but the E_c values were not found to be significantly sensitive to the magnitude of ξ. The results indicate that both H–S and H–T modeling could not account for the high modulus of elasticity observed in the experiments around a PEPEG content of 7 wt.%. This difference in the experimental and theoretical magnitude of E_c is due to the fact that the structural changes in the silica network on addition of PEPEG oligomer have not been taken into account by these computational models. Further research is needed to develop modeling of deformations in such porous composites and to explain the deviations from the experimental results due to microstructural alterations.

Meador et al. [27] have also reported an optimum in the elastic modulus with epoxy loading, for an epoxy-crosslinked, amine-modified silica aerogel. Those authors argued that the epoxy bridges the neighboring amine-modified silica clusters and hence increases the strength of the aerogels. However, they also observed that maximum strength is obtained for a moderate extent of modification by amine and epoxy. The latter effect arises due to the fact that after a certain amount of addition of epoxy, it is further bonded to the same amine site on the silica cluster. However, in our work, as shown in Eq. (3) and discussed earlier, since the PEPEG has only one reactive –OH group, it cannot bridge the neighboring silica chains. This is in contrast to polymers having two functional groups, as in the case of the epoxy-cross-linked aerogels of Meador et al. [27].

Novak et al. [28] reported in situ addition of linear poly(2-vinylpyridine) (PVP) polymer, during silica gel matrix formation. They argued that this resulted in hydrogen bond formation between surface silanol groups of silica with the nitrogen atom of the pyridine groups in PVP. Hydrogen bond formation was hypothesized based on negligible leaching of PVP during subsequent solvent exchange of the gel composite, confirming that PVP was more than just physically mixed with silica. Similarly, in our experiments, it is possible that multiple oxygen atoms in a PEPEG chain can form hydrogen bonds with surface silanol groups of silica. This may lead to a bridging of silica particles by PEPEG chains.

Therefore, based on our observations, PEPEG at low loading (<7 wt.%) reinforces the silica matrix via pore filling and partitioning into the neck region of silica particles. At higher PEPEG content (>7 wt.%), the steric hindrance of the PEPEG to the backbone silica matrix formation becomes dominant and hence the elastic modulus decreases.

Interestingly, it was observed that with the increase in PEPEG from 0 wt.% (pure silica) to 10 wt.%, the toughness of the composites increased proportionately from 0.01 to 0.08 J (Fig. 8), even though elastic modulus decreased above 7 wt.% PEPEG. This is because the oligomers trapped in the silica network can sustain higher strain values as compared to the pure silica network as seen from Fig. 9. The strength (i.e. breaking stress) of pure silica is slightly smaller as compared to the silica–PEPEG composites. As the amount of PEPEG increases from 0 to 7 wt.%, the breaking stress increases from 1 to 2.5 MPa. From the TMAFM and BET measurements it was observed that, for PEPEG < 7 wt.%, the oligomer fills some of the pores and neck region between the silica particles, which strengthens the composite matrix. However, on further increase in PEPEG, the breaking stress decreased to 2.3 because of the structural changes taking place in the composites as discussed earlier.

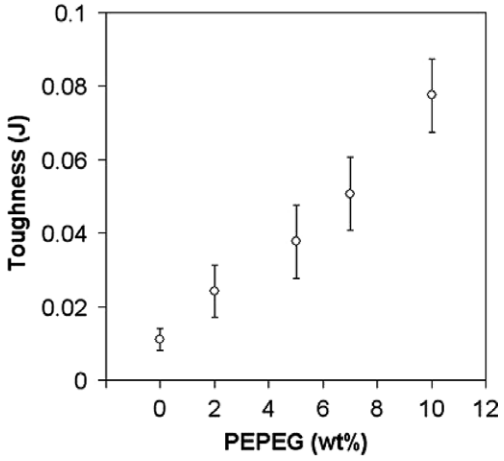

Fig. 8. Toughness of the silica–PEPEG composite xerogels as a function of PEPEG (wt.%) determined by area the under the stress–strain curve. The errors are estimated from measurements of four different samples of identical composition.

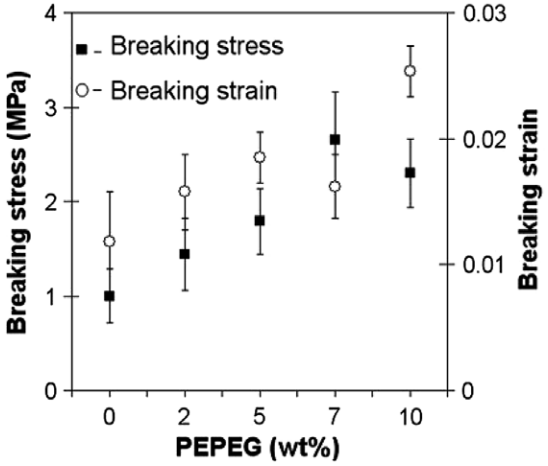

Fig. 9. Breaking stress and strain of the silica–PEPEG composite xerogels as a function of PEPEG (wt.%). The errors are estimated from measurements of at least four different samples of identical composition.

Fig. 10 shows Vickers hardness of the xerogel samples determined from microhardness measurements for test loads of 50 and 100 gf. The measured hardness is independent of the applied load; but has a large variation across different samples with the same composition, which is due to the non-uniformity in the microstructure of the xerogel composites. It can be broadly concluded that Vickers hardness increases from 7.3 to 16 Mdyn/mm^2 with an increase in PEPEG from 0 to 5 wt.%, but decreases marginally to an average value of 14 Mdyn/mm^2 on further PEPEG addition. For PEPEG up to 5–7 wt.%, the oligomer fills the small pores leading to a decrease in the void volume, and hence the indentation depth also decreases. However, with further increase in PEPEG, the composite network becomes more porous. This shift towards larger pore size and reduced cross-linking between silica particles leads to decreased microhardness. A similar trend was observed by Jung et al. [29] in the case of silica–PEG sonogels, where the microhardness increased from 70 to 90 Mdyn/mm^2 with an increase in PEG from 0 to 10 wt.% and then decreased to 10 Mdyn/mm^2 with further increase in PEG to 40 wt.%.

A similar optimum was also observed in the structural loss factor studies as seen from Fig. 11. For the vibration damping tests [30], an aluminum bar of dimensions 50 cm × 2.5 cm × 0.2 cm was used as a cantilever beam base for pasting the silica–PEPEG composite xerogel sample. A sample of dimensions 3 cm × 2.5 cm × 0.4 cm was pasted at a distance of 5 cm from the fixed end of the cantilever using a very thin layer of epoxy glue. To record the amplitude of the beam, a piezoelectric sensor (bimorph) was pasted at the opposite side of the beam below the xerogel sample and its output waveform was recorded using a sensitive digital oscilloscope. The free end of the cantilever was deflected through a predetermined distance of 3 mm and left free to oscillate. The damping behavior of the beam with and without pasted samples was analyzed. The logarithmic decrement (δ) in amplitude of the beam was calculated from amplitude decrement in the first (d_1) and nth peak (d_n) as per the following equation [31]:

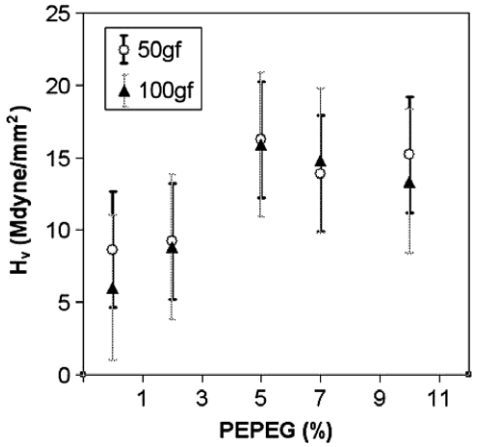

Fig. 10. Vickers hardness of silica–PEPEG composites. The errors are estimated from measurements of three different samples of identical composition.

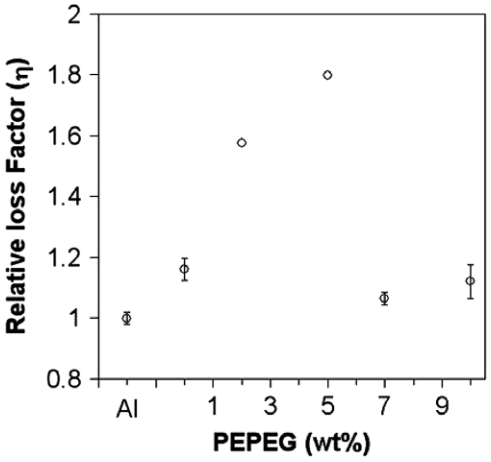

Fig. 11. Relative loss factor as a function of PEPEG (wt.%). The loss factor of Al beam was considered as reference and accordingly the other values are plotted. The errors are estimated from measurements of three different samples of identical composition.

$$\delta = (1/n)\ln(d_1/d_n) \tag{10}$$

This logarithmic decrement is directly related to the loss factor (η) ≅ δ/π.

As only 6% of the Al beam was covered by the xerogel sample during the measurements, the Al beam loss factor is treated as 1 and the structural loss factor of the Al beam and xerogel composite system was calculated relative to this. Fig. 11 shows that the structural loss factor is optimum for composites with 5 wt.% PEPEG.

4. Conclusions

Silica–PEPEG oligomer nanocomposite xerogels of different oligomer concentrations were prepared by sol–gel processing and the microstructure was related to measured mechanical properties. Addition of PEPEG oligomer to the silica xerogel causes a twofold decrease in BET specific surface area as the oligomer fills the pores in the silica matrix. Therefore, with increasing PEPEG content, the pore size distribution shows a decreasing number of smaller pores because these are filled. Simultaneously, a higher number of larger pores appear because with increasing fraction of oligomer, it partitions more in the silica matrix rather than in the pores. FTIR spectral data support this structural transition by showing an increase in the magnitude of absorption bands corresponding to C–H and a decrease in the magnitude of the bands related to Si–O–Si, which indicates partial disruption of silica network formation. Topographic and phase images obtained using TMAFM conclusively prove that the oligomer initially fills the pores, but its increased fraction forces penetration in the ''neck'' region between the silica particles. It is also observed from the AFM scans that both the average pore and particle size increase with increasing oligomer concentration. These results are attributed to the formation of only a partially cross-linked network of silica due to the steric hindrance of PEPEG chains, which is significant for PEPEG > 7 wt.%.

With an increase in PEPEG, on the other hand, the toughness of the composite increases monotonically as the oligomer chains can sustain higher strain values. However, the measured compressive Young's modulus increases from ~87 MPa for pure silica to ~157 MPa for 7 wt.% PEPEG and decreases again to ~98 MPa with further addition of PEPEG. This is because of the microstructural changes discussed above. The proof of these structural changes in the composite is also reflected in its Vickers hardness and structural loss factor values. For example, the Vickers hardness initially increases from 10 to 20 $Mdyn/mm^2$ with an increase in PEPEG from 0 to 5 wt.%, but slightly decreases with further addition of PEPEG. The structural loss factor of an Al beam covered by a small xerogel sample almost doubled with an increase in PEPEG from 0 to 5 wt.%, but decreased with a further increase in PEPEG beyond this range. These observations suggest that the PEPEG–silica nanocomposite has an optimal mechanical reinforcement of silica network at around 7 wt.% PEPEG. This is the maximum PEPEG fraction at which the oligomer continues to mechanically reinforce the silica matrix without disrupting and weakening its cross-linking significantly.

The H–S analytical model and H–T empirical model cannot explain a rapid increase of modulus near 7 wt.% PEPEG and its subsequent decline thereafter because of network disruption. Thus, the predictions of theory and its underlying physics are valid only for lower (<7 wt.%) PEPEG fraction. This is due to the fact that these models do not incorporate the effects of the significant structural changes witnessed in our composites around 7 wt.%. This clearly underlines the need for a more general model that incorporates the structural changes for improved prediction of various composite properties.

Acknowledgement

This work was supported by the DST unit on Nano Science and Technology at IIT, Kanpur.

Appendix A. Supplementary data

Supplementary data associated with this article can be found, in the online version, at doi:10.1016/j.actamat.2006.06.055.

References

[1] Guo L, Hyeon-Lee J, Beaucage G. J Non-Cryst Solids 1999;243:61.
[2] Hu X, Littrel K, Ji S, Pickles DG, Risen Jr WM. J Non-Cryst Solids 2001;288:184.
[3] Martin J, Hosticka B, Lattimer C, Norris PM. J Non-Cryst Solids 2001;285:222.
[4] Guha P, Ganguli D, Chaudhuri S, Chakrabarti K. Mater Lett 2004;58:2963.
[5] Nishio K, Okubo K, Watanabe Y, Tsuchiya T. J Sol–Gel Sci Technol 2000;19:187.
[6] Chawla N, Sidhu RS, Ganesh VV. Acta Mater 2006;54:1541.
[7] Halpin JC, Tsai SW. Air Force Mater Lab 1967:423. TR 67.
[8] Hashin Z, Shtrikman S. J Mech Phys Solids 1963;11:127.
[9] Pundale SH, Rogers RJ, Nadkarni GR. AFS Trans 1998;102:98.
[10] Thostensen ET, Chou TW. J Phys D Appl Phys 2003;36:573.
[11] Fornes TD, Paul DR. Polymer 2003;44:4993.
[12] Pierre AC. Introduction to sol–gel processing. Massachusetts: Kluwer Academic; 1998.
[13] Floess JK, Field R, Rouanet S. J Non-Cryst Solids 2001;285:101.
[14] Leventis N, Sotiriou-Leventis C, Zhang G, Rawashdeh A-M. Nano Lett 2002;2:957.
[15] Modern plastic encyclopedia, vol. 43, no. 1A. New York (NY): McGraw-Hill; 1965. pp. 28.
[16] Hæreid S, Dahle M, Lima S, Einarsrud M-A. J Non-Cryst Solids 1995;186:96.
[17] Venkateswara Rao A, Bhagat SD. Solid State Sci 2004;6:945.
[18] Kim SM, Chakrabarti K, Oh EO, Whang CM. J Sol–Gel Sci Technol 2003;27:149.
[19] Barral K. J Non-Cryst Solids 1998;225:46.
[20] Smith DM, Scherer GW, Anderson JM. J Non-Cryst Solids 1995;188:191.
[21] Aelion R, Loebel A, Eirich F. J Am Chem Soc 1950;72:5705.
[22] (a) Brinker CJ, Scherer GW. In: Sol–gel science. San Diego (CA): Academic Press; 1990. p. 523;
(b) Brinker CJ, Scherer GW. In: Sol–gel science. San Diego (CA): Academic Press; 1990. p. 360.
[23] Jeong Ae-Y, Goo S-M, Kim D-P. J Sol–gel Sci Technol 2000;19:483.
[24] Iler RK. The chemistry of silica. New York (NY): John Wiley; 1979. p. 222.
[25] Wall P. Appl Mathemat 1997;42:245.
[26] Hui CY, Shia D. Polymer Eng Sci 1998;38:774.
[27] Meador MA, Fabrizio EF, Ilhan F, Dass A, Zhang G, Vassilaras P, et al. Chem Mater 2005;17:1085.
[28] Novak BM, Auerbach D, Verrier C. Chem Mater 1994;6:282.
[29] Jung HY, Gupta HY, Seo DW, Kim YH, Whang CM. Bull Korean Chem Soc 2002;23:884.
[30] Suhr J, Koratkar N, Ajayan P. Proc SPIE 2004;5386:153.
[31] Thomson WT. Vibration theory and applications. Prentice-Hall; 1965. p. 45.